Journal of Digital Imaging (2022) 35:846–859
https://doi.org/10.1007/s10278-022-00592-0

ORIGINAL PAPER

Computer-Aided Diagnosis for Determining Sagittal Spinal Curvatures Using Deep Learning and Radiography

Hyo Min Lee[1] · Young Jae Kim[1] · Je Bok Cho[2] · Ji Young Jeon[3] · Kwang Gi Kim[4,5]

Received: 25 May 2021 / Revised: 17 January 2022 / Accepted: 18 January 2022 / Published online: 11 March 2022
© The Author(s) under exclusive licence to Society for Imaging Informatics in Medicine 2022

Abstract

Analyzing spinal curvatures manually is time-consuming and tedious for clinicians, and intra-observer and inter-observer variability can affect manual measurements. In this study, we developed and evaluated the performance of an automated deep learning–based computer-aided diagnosis (CAD) tool for measuring the sagittal alignment of the spine from X-ray images. The CAD system proposed here performs two functions: deep learning–based lateral spine segmentation and automatic analysis of thoracic kyphosis and lumbar lordosis angles. We utilized 322 datasets with data augmentation for learning and fivefold cross-validation. The segmentation model was based on U-Net, which has multiple applications in medical image processing. Here, we utilized parameter equations and trigonometric functions to design spinal angle measurement algorithms. The kyphosis (T4–T12) and lordosis angle (L1–S1, L1–L5) were automatically measured to help diagnose kyphosis and lordosis. The segmentation model had precision, sensitivity, and dice similarity coefficient values of $90.53 \pm 4.61\%$, $89.53 \pm 1.8\%$, and $90.22 \pm 0.62\%$, respectively. The performance of the CAD algorithm was also verified with the Pearson correlation, Bland–Altman, and intra-class correlation coefficient (ICC) analysis. The proposed angle measurement algorithm exhibited high similarity and reliability during verification. Therefore, CAD can help clinicians in reaching a diagnosis by analyzing the sagittal spinal curvatures while reducing observer-based variability and the required time or effort.

Keywords Deep learning · Segmentation · Computer-aided diagnosis · Thoracic kyphosis · Lumbar lordosis

Introduction

Spine, an important anatomical structure in the human body, is a complex multi-articular system that supports the head and half of the body weight and protects the spinal cord, spinal nerve roots, and vertebral arteries [1]. The normal physiological curvature of the spine consists of a series of harmonious curves in the sagittal plane: cervical lordosis, thoracic kyphosis, and lumbar lordosis [2].

Previous studies suggest that increase in thoracic curvature is associated with back pain and higher risk of fracture, as well as a lower quality of life. Furthermore, decreased lumbar lordosis is also associated with back pain, higher fall risk or loss of balance, and lower quality of life. Therefore, spinal deformity with back pain due to spinal cord injury, weakness, metastatic disease of the spine, and degenerative spine disease etc. can lead to a decrease in the quality of life [3–5].

The growing elderly population and the practice of fixed regular stances for prolonged durations contribute to a rise in the number of spinal deformity cases [6, 7]. According

✉ Ji Young Jeon
mdjeonjy@gmail.com

✉ Kwang Gi Kim
kimkg@gachon.ac.kr

1 Department of Biomedical Engineering, College of Health Science, Gachon University, Seongnam, South Korea

2 Department of Medical Devices Convergence Center, Gachon University, Seongnam, South Korea

3 Department of Radiology, Gil Medical Center, Gachon University College of Medicine, 21, Namdong-daero 774 beon-gil, Namdong-gu, Incheon 21565, Republic of Korea

4 Department of Health Sciences and Technology, Gachon Advanced Institute for Health Sciences and Technology (GAIHST), Gachon University, Seongnam, South Korea

5 Department of Biomedical Engineering, Gil Medical Center, Gachon University College of Medicine, 21, Namdong-daero 774 beon-gil, Namdong-gu, Incheon 21565, Republic of Korea

to the World Health Organization (WHO) survey, between 250,000 and 500,000 people suffer a spinal cord injury each year. Additionally, spinal deformity is reported as a serious condition in elderly individuals with degenerative changes in the spine and adolescents who have prolonged improper postures [8–10].

Radiological analysis of spinal curvature is utilized to evaluate various spinal disorders. Spinal curvature analysis is important in clinical decisions and research development. In clinical practice, a treatment modality is usually determined based on the degree of abnormal curvature and progression of deformity. However, in research, spinal curvature is assessed to evaluate treatment outcomes, and effectiveness of interventional studies.

A diverse range of non-invasive measurement devices (e.g., the flexicurve and the manual inclinometer) facilitate the measurement of spinal posture in clinical practice. In particular, the Cobb angle technique using radiographic images is considered the gold standard for postural assessment of the spine in the sagittal plane [11–13].

Since the radiographic angle for acquiring X-ray images is assessed manually, variability in the measurement value may occur even when measured by the same operator [14]. The technical quality of the radiograph that is affected by intra-observer and inter-observer variability influences the clinician's interpretation [15].

Due to the growing demand for precise measurement of spinal angles, computer-aided diagnosis (CAD) has shown significant progress [16–20]. Al Arif et al. (2018) performed automatic segmentation of cervical spine X-ray images with a novel shape-aware deep segmentation network (Unet-S) and a U-Net model. Here, the authors could achieve a dice similarity coefficient (DSC) of 0.84 and an average shape error of 1.69 mm [21]. Moreover, U-Net and web-based spine segmentation in computed tomography images provides DSC and sensitivity values of 90.4% and 86.99%, respectively [22]. Additionally, digitalized video fluoroscopic imaging (DVFI) system with Siamese convolutional network can automatically track lumbar vertebra with rotated bounding boxes [23]. Alternately, a sequential conditional reinforcement learning network (SCRL) can detect and segment vertebral bodies simultaneously from magnetic resonance (MR) spine images with a DSC of 92.6% [24].

A CAD system can automatically analyze Cobb's angle using an active shape model to provide a diagnosis for scoliosis. Spine angle measurements in anteroposterior (AP) X-ray image had a tolerance of 3–4 degrees in comparison to experts' measurements [25]. Deep learning convolutional neural network (CNN) approaches like U-Net, dense U-Net, and residual U-Net can be utilized to automatically measure spinal curvatures from anterior–posterior (AP) view of spinal X-ray images. The developed system provides a complete segmented spine image along with accurate spine curvature measurements to aid in clinical diagnosis [26]. Yet another automatic measurement method utilized trigonometric functions to measure Cobb's angle, and the ResNet-50 convolution neural network (CNN) detected vertebra within ~ 15° of the surgeons' measurements [27].

Therefore, automatic segmentation and measurement of Cobb's angle in AP image for scoliosis diagnosis is well established. However, not only there have been very few reports analyzing sagittal spinal angles, but also previous studies are semi-automatic systems that require radiologists to participate in measurements. Therefore, the CAD system that fully automatically analyzes kyphosis and lordosis has not been reported yet. In this study, we performed lateral (LAT) spine segmentation using U-Net, which is a deep learning model in CNN that can segment medical images [28]. Furthermore, we proposed a fully automated CAD system based on deep learning to measure kyphosis and lordosis angles. Our CAD system based on deep learning should minimize observer variability in comparison with manual measurement, and be cost-effective, time-efficient, reliable, and reproducible.

Materials and Methods

Dataset Collection

A total of 322 whole spine LAT X-ray images formatted with digital imaging and communications in medicine (DICOM) were collected from Gil Hospital with IRB approval (IRB number: GDIRB2019-137). Data of adult patients diagnosed with scoliosis with an average age of 62 years (standard deviation: ± 15) was considered. The datasets include examples of vertebrae with catheters, degenerative changes, and bone implants. All data were anonymized, and standard research protocols have been followed. Two experts who were trained to identify vertebrae for radiologists demarcated the region of interest (ROI) on the LAT spine images using ImageJ (NIH, Bethesda, MD, USA). The final ROI was determined after revision and modification by two radiologists with more than 10 years of experience.

Development Environment

The deep learning model for spine lateral segmentation was implemented on Ubuntu (18.04) operating system using Python (3.6.1), Keras (2.3.1), and TensorFlow. For the development of kyphosis and lordosis measurement CAD system, Microsoft visual studio (version 2017, Microsoft, Redmond, WA, USA), insight toolkit (ITK, version 4.4.1; Insight Segmentation and Registration Toolkit, Kiteate Inc., NY, USA) [29], and visualization toolkit (VTK, version 5.10.0) [30] were used.

Data Pre-processing

For deep learning, all the input data must have the same size. Resizing and zero-padding were applied to all the input images to set the size as 1024 × 1024 pixels with a value of 8 bits per pixel. To prevent overfitting during training, and to improve the network performance, data augmentation was used for the training data [31]. Four transformed images were produced from one training image by applying rotation of approximately 15° and space augmentation or shifting translation of around 5%. Thus, 968 training images were generated with data augmentation, and the remaining 60 test images were used for verification. We trained the model by fivefold cross-validation to determine the model's performance quantitatively.

U-Net Architecture

To capture vertebral features, the U-Net algorithm optimized for medical image segmentation was implemented [32]. U-Net consists of a contraction path to extract image features, an expansion path to expand the feature map size, and skip-connections to minimize information loss and perform accurate localization (Fig. 1). Rectified linear unit (ReLu) function was used as the activation function, while the sigmoid function was utilized in the last convolutional layer. The hyperparameter was set as 4 batch size, 100 epochs, and 0.001 learning rate. Additional information of the U-Net algorithm is presented in Table 1.

Data Post-processing

If the result mask images contain pieces of noise from lumbar implant, medical catheter, or thick adipose tissue etc., data post-processing is required to remove the noisy elements. Mis-detection of the noise as a vertebral body obscures angle measurement. Thus, morphology post-processing, which includes erosion and dilation, was used to minimize noise. Erosion is the process of peeling an image; when the pixel kernel overlays noise smaller than the kernel, 1 is updated to 0. Dilation is an expansion process that alters the perimeter; when the noise does not completely overlap with the kernel, 0 is flipped to 1. The erosion and dilation processes were applied twice to the predicted image by the segmentation model using a 4 × 4 kernel (Fig. 2).

Measurement of Spinal Curvature (Sagittal Alignment of the Spine)

Thoracic kyphosis and lordosis are diagnosed using an image of the lateral spine in the sagittal plane. Figure 3

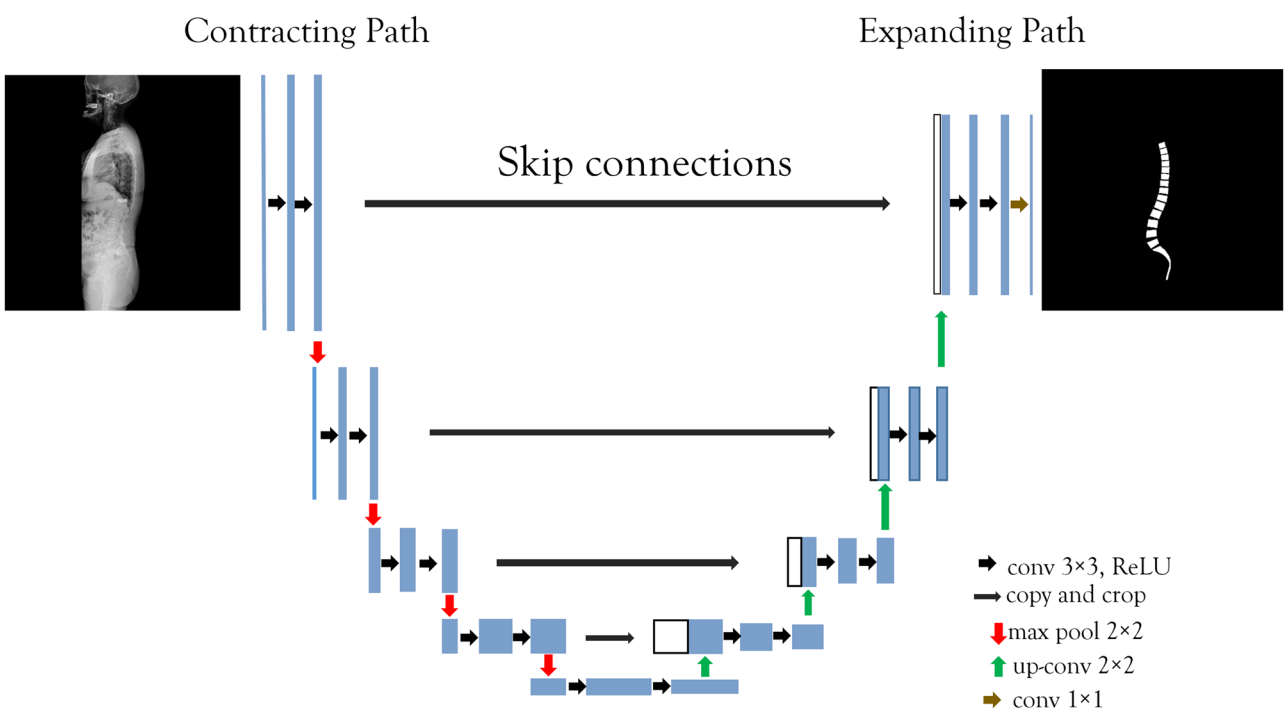

Fig. 1 U-Net architecture for training the segmentation model

Table 1 The network structure and hyperparameters of U-net

	Unit level	Conv layer	Filter	Activation function	Output size
Input					1024 × 1024 × 1
Encoding	Level 1	Conv 1	3 × 3 / 32	ReLu	1024 × 1024 × 32
		Conv 2	3 × 3 / 32		1024 × 1024 × 32
	Level 2	Conv 3	3 × 3 / 64	ReLu	512 × 512 × 64
		Conv 4	3 × 3 / 64		512 × 512 × 64
	Level 3	Conv 5	3 × 3 / 128	ReLu	256 × 256 × 128
		Conv 6	3 × 3 / 128		256 × 256 × 128
	Level 4	Conv 7	3 × 3 / 256	ReLu	128 × 128 × 256
		Conv 8	3 × 3 / 256		128 × 128 × 256
Bridge	Level 5	Conv 9	3 × 3 / 512	ReLu	64 × 64 × 512
		Conv 10	3 × 3 / 512		64 × 64 × 512
Decoding	Level 6	Conv 11	3 × 3 / 256	ReLu	128 × 128 × 256
		Conv 12	3 × 3 / 256		128 × 128 × 256
	Level 7	Conv 13	3 × 3 / 128	ReLu	256 × 256 × 128
		Conv 14	3 × 3 / 128		256 × 256 × 128
	Level 8	Conv 15	3 × 3 / 64	ReLu	512 × 512 × 64
		Conv 16	3 × 3 / 64		512 × 512 × 64
	Level 9	Conv 17	3 × 3 / 32	ReLu	1024 × 1024 × 32
		Conv 18	3 × 3 / 32		1024 × 1024 × 32
Output		Conv 19	1 × 1	Sigmoid	1024 × 1024 × 1

summarizes the measurements of spinal curvatures in the sagittal plane. Thoracic kyphosis is evaluated by measuring the angular intersection between lines parallel to the T4 superior and the T12 inferior end plate [33]. Lumbar lordosis is the angular intersection between lines parallel to the superior end plate of L1 and the sacrum superior (S1). Some radiologists measure the angular intersection between lines parallel to the L1 superior and the L5 inferior end plate as needed (e.g., when the sacrum is not visible on the X-ray image) [34, 35]. Here, we measured thoracic kyphosis based on T4–T12 and lumbar lordosis based on L1–S1 and L1–L5.

Algorithm for Kyphosis and Lordosis Angle Measurement

The developed CAD system follows the algorithm outlined in Fig. 4. First, the system receives the formatted DICOM files as input, and then, a trained segmentation model determines the vertebral contour. Second, angles of kyphosis and lordosis are estimated. Third, the measured angles are visualized by overlaying it with the original X-ray image.

The vertebral contour is detected from the previously learned segmentation model. As shown in Fig. 5a, the CAD system detects the vertebral body contours.

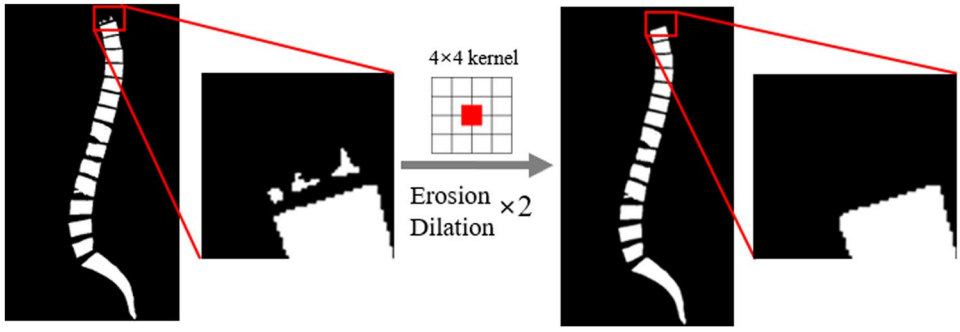

Fig. 2 Data processing for deep learning

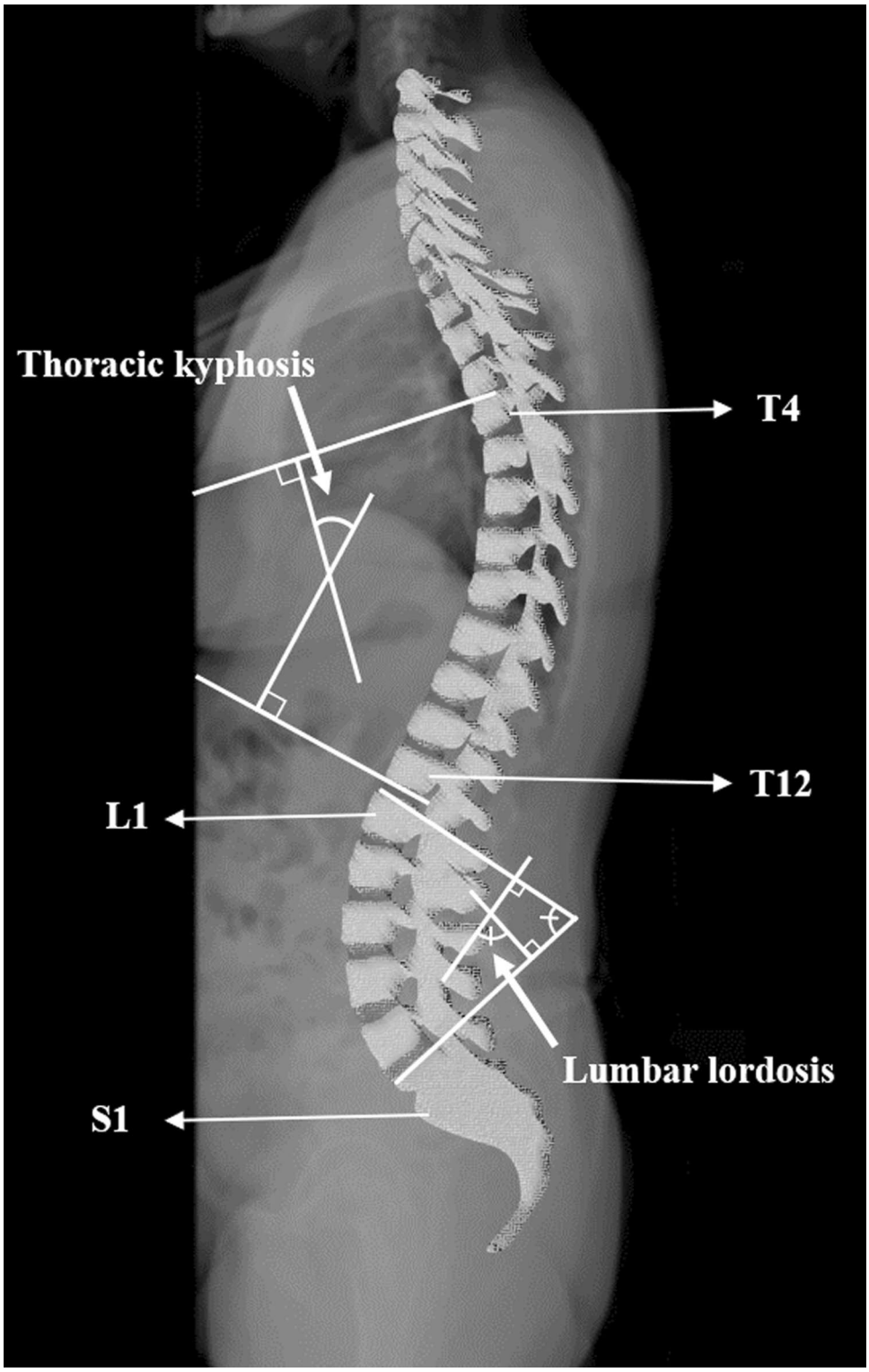

Fig. 3 Measurement of thoracic kyphosis and lumbar lordotic angles using Cobb's method in a lateral radiographic image of the spine

A minimal bounding box was generated to circumscribe the vertebral body contour. Since the order in which the vertices of the box are generated varies based on the slope of the vertebral body, exception processing was performed such that vertices are generated in the same order. Figure 5b depicts the upper plate and the end plate of the vertebral body, and based on the parameters, the straight-line equations are calculated as follows.

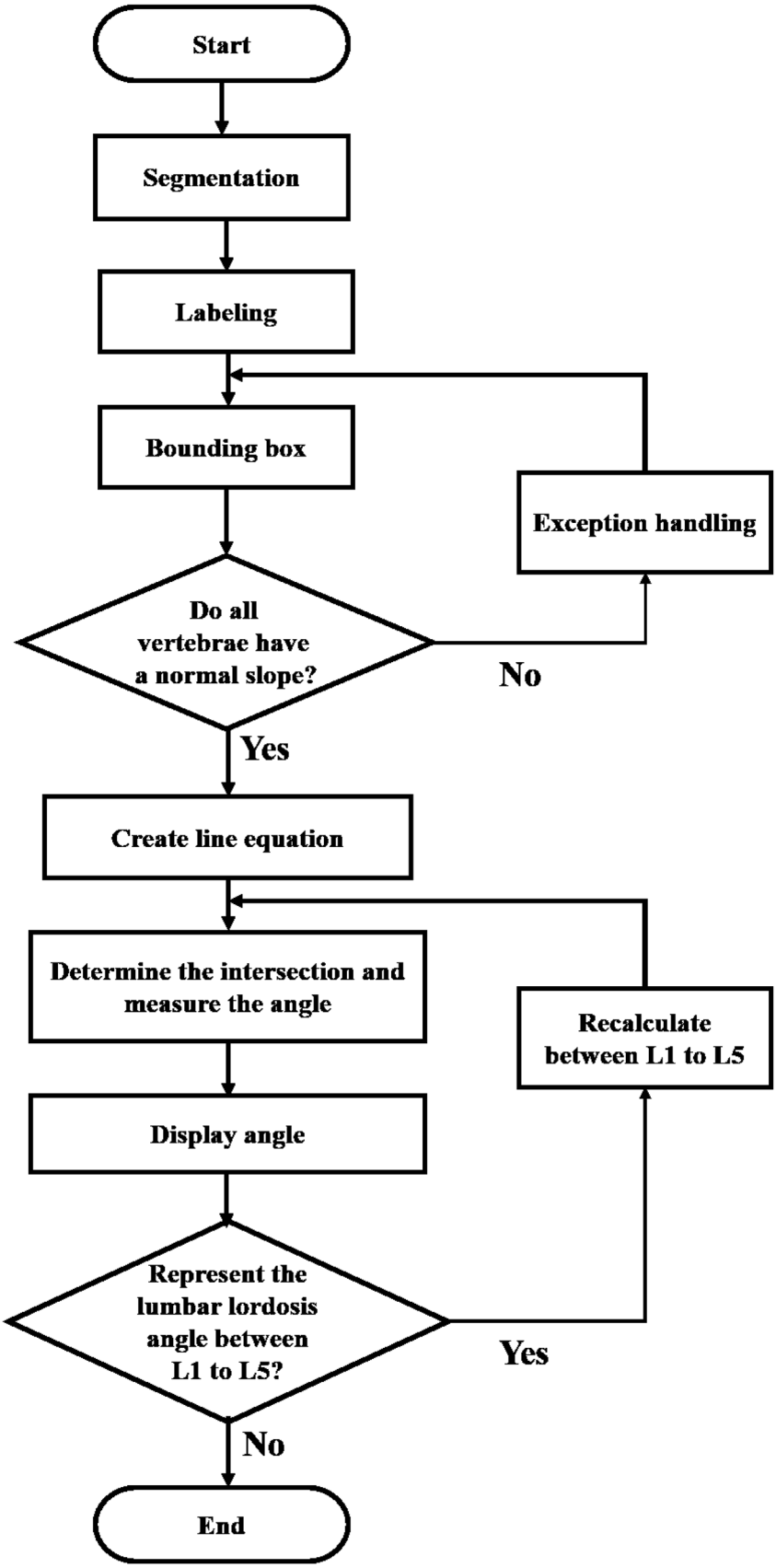

Fig. 4 Automated CAD system algorithm

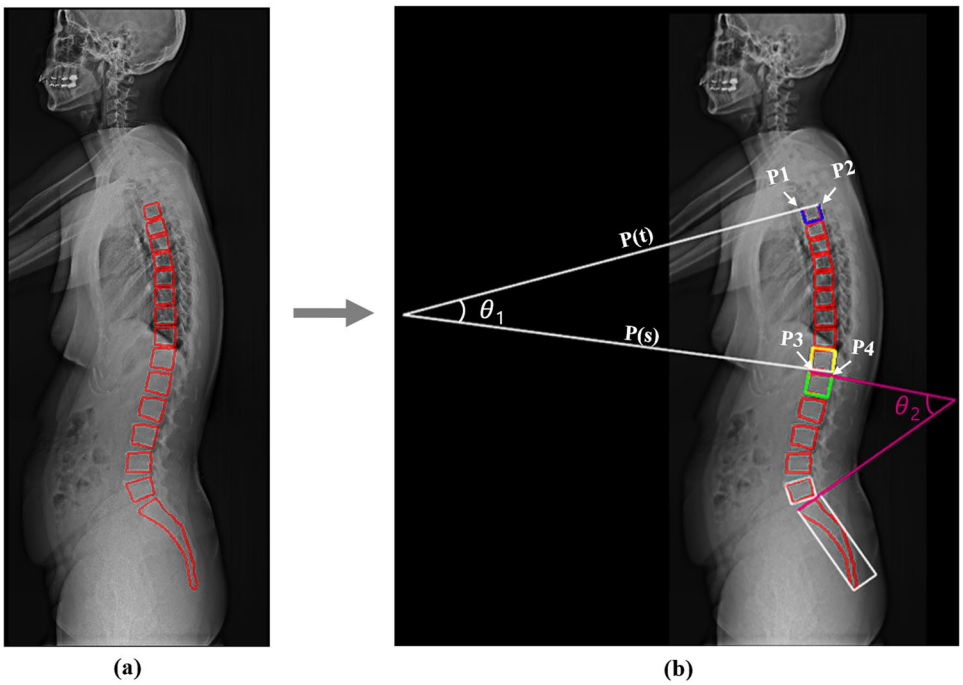

Fig. 5 Measurement process for kyphosis and lordosis angles in the CAD program. **a** Predicted contours of the whole spine vertebrae from the deep learning model. **b** Equation parameters and the vertebral body coordinates with the bounding box

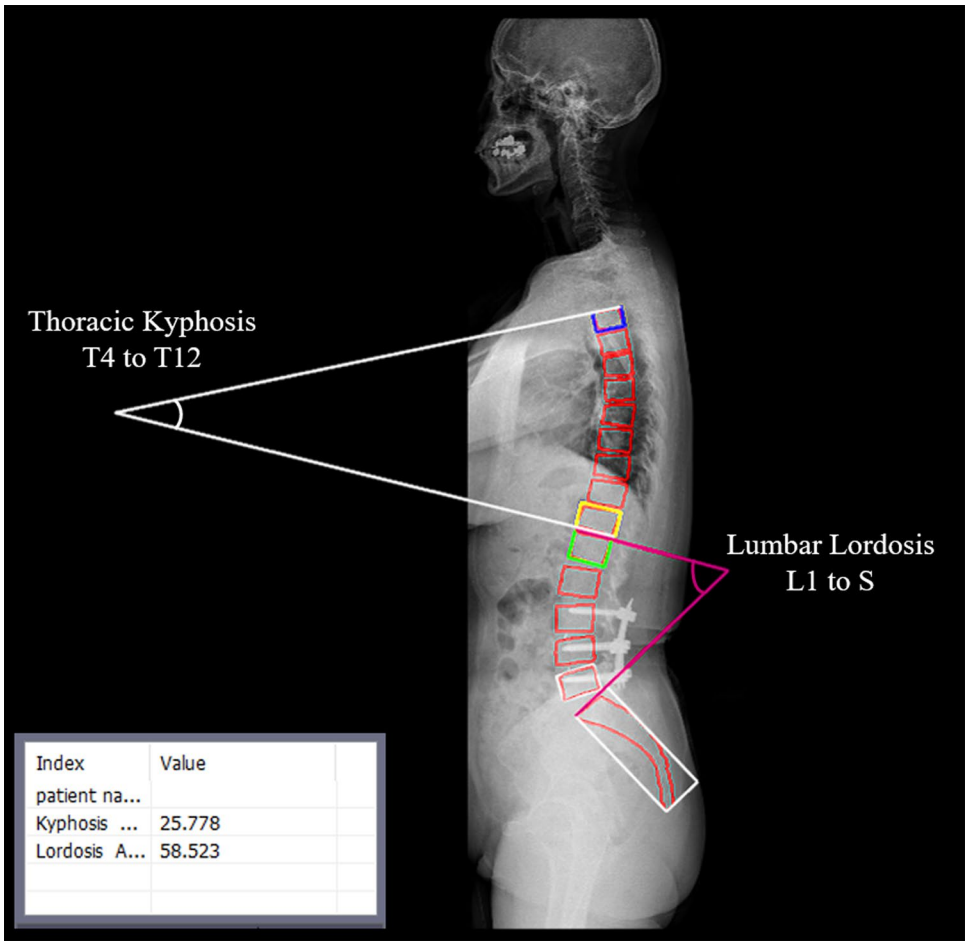

Fig. 6 Representative analysis result from the CAD program. The thoracic kyphosis and lumbar lordosis (L1–S) angles are depicted on the image and the values are displayed below

$$P(t) = (1 - \mathrm{t})P_1 + tP_2, \tag{1}$$

$$P(s) = (1 - \mathrm{s})P_3 + sP_4, \tag{2}$$

where t and s are parameters, $P(t)$ and $P(s)$ are equations of a straight line, and P_1, P_2, P_3, and P_4 are the coordinates of the vertices of the vertebral body. The simultaneous straight-line equations determine the coordinates of the intersection of the upper plate and the end plate. The angle between the intersection and vertebrae is determined as follows.

$$\theta_1, \theta_2 = \cos^{-1}\frac{b^2 + c^2 - a^2}{2bc}, \tag{3}$$

where θ_1, θ_2 represents the angle between the two straight lines; a, b, and c represent the distance between the coordinates of the three points. The angle between T4 and T12 is the thoracic kyphosis, and the angle between L1 and L5 or L1 and S1 is the lumbar lordosis.

Statistical Analysis

We assessed the segmentation model performance by comparing the segmented images with the ground truth pixel by pixel. Three evaluation criteria—precision, sensitivity, and DSC—were utilized. Cases in which the vertebrae were recognized as vertebrae were considered true positive (TP), whereas if the non-vertebrae regions were recognized as vertebrae, they were classified as false positive (FP). Furthermore, true negative (TN) implied that non-vertebrae regions were recognized as non-vertebrae, and false negative (FN) implied that vertebrae were incorrectly recognized as non-vertebrae. Precision, sensitivity, and DSC were determined using Eqs. (4)–(6).

$$\text{Precision} = \frac{\text{TP}}{\text{TP} + \text{FP}} \tag{4}$$

$$\text{Sensitivity} = \frac{\text{TP}}{\text{TP} + \text{FN}} \tag{5}$$

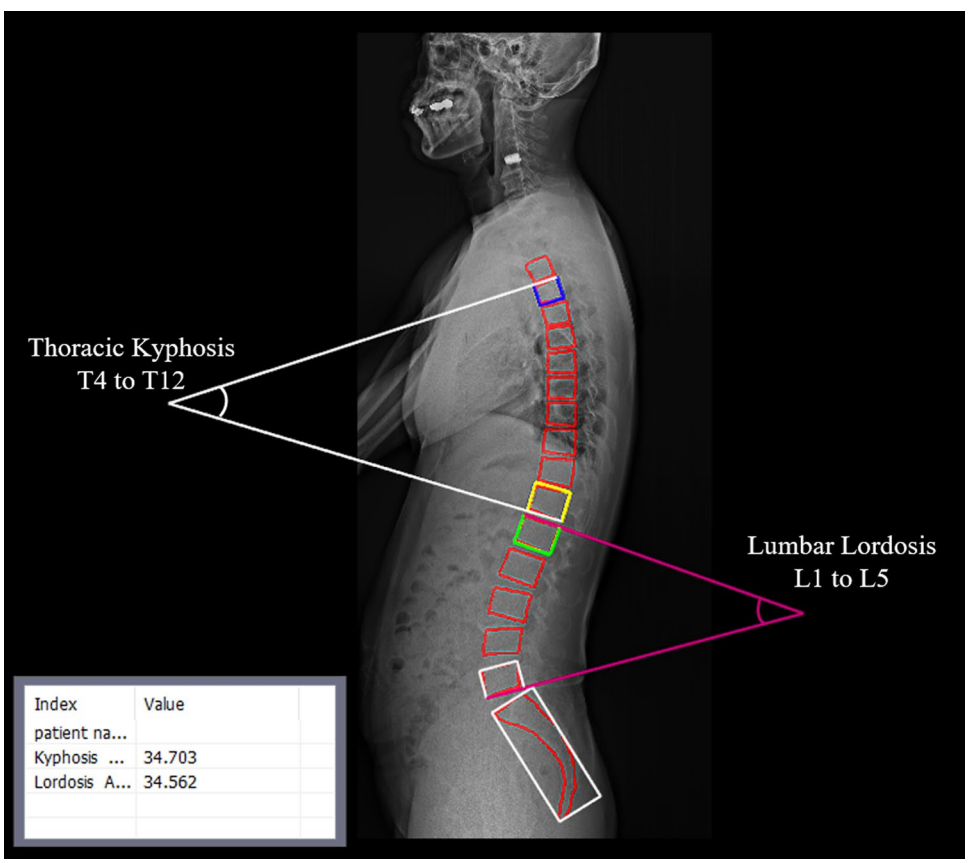

Fig. 7 Representative result from CAD program, where thoracic kyphosis and lumbar lordosis were measured based on L1–L5. The measured angle values are depicted on the bottom left

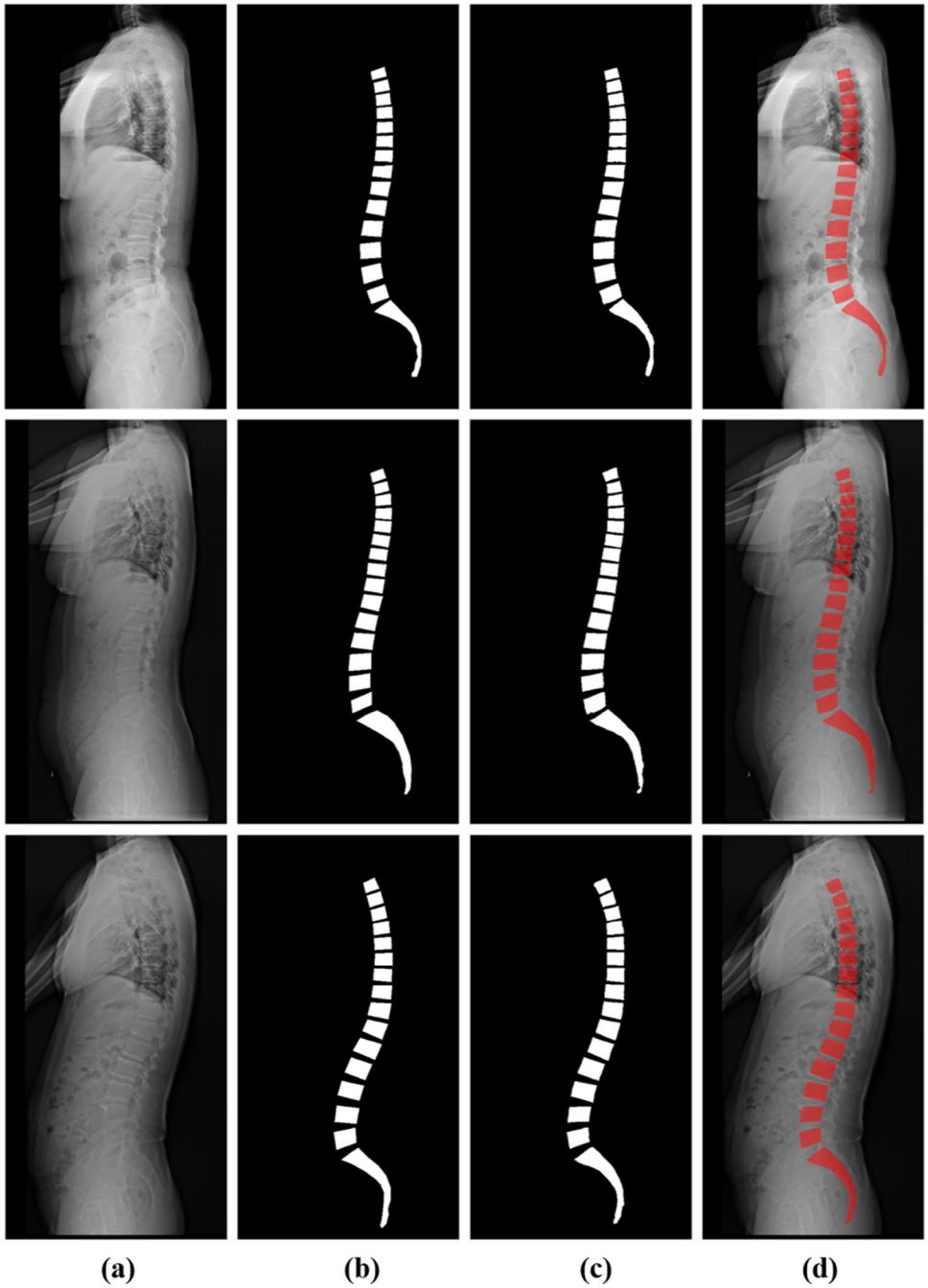

Fig. 8 Resulting images of segmentation of whole lateral spine. **a** Original images. **b** Ground truth images. **c** Segmentation result images. **d** Overlaid images

$$\mathrm{DSC} = \frac{\mathrm{TP}}{(\mathrm{TP}+\mathrm{TN})+(\mathrm{FP}+\mathrm{FN})} \times 2 \tag{6}$$

The performance of the CAD algorithm was verified with Pearson correlation, intra-class correlation coefficient (ICC) analysis, and Bland–Altman plot using MedCalc 19.7 (MedCalc Software, Ostend, Belgium) program. Pearson correlation analyzes linear or nonlinear relationships between two variables using a correlation coefficient (R). The value of R ranges between –1 and 1, where –1 denotes negative correlation, 1 denotes positive correlation, and

Table 2 Five-fold cross-validation results of the trained segmentation model

Cross-validation number	Precision (%)	Sensitivity (%)	DSC (%)
1	89.92	86.04	89.14
2	92.95	91.29	91.02
3	89.70	89.92	90.24
4	83.01	89.95	90.54
5	97.08	90.47	90.17
Average	90.53 ± 4.61	89.53 ± 1.8	90.22 ± 0.62

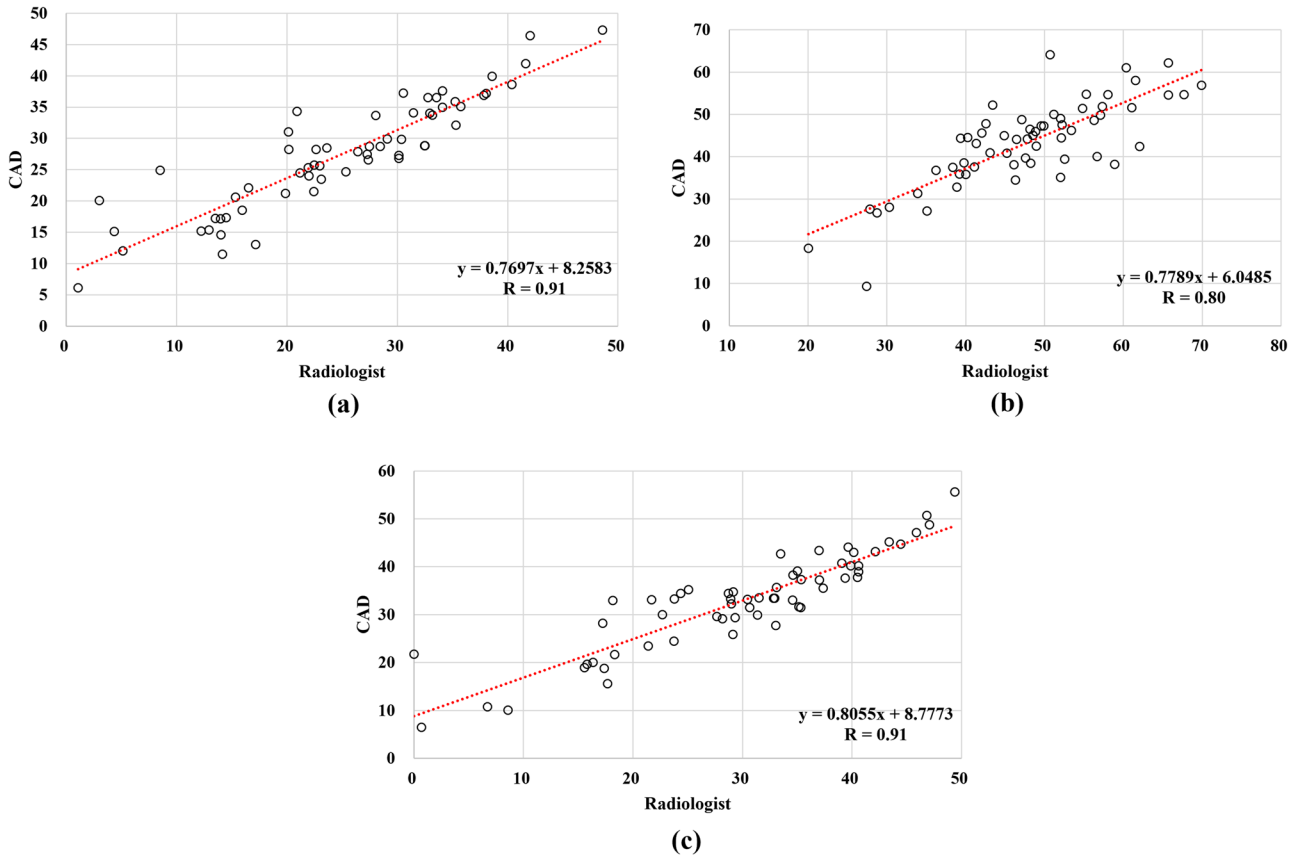

Fig. 9 Scatter chart plots comparing angles measured by radiologist and the CAD system. **a** Thoracic kyphosis. **b** Lumbar lordosis based on L1–S. **c** Lumbar lordosis based on L1–L5

0 indicates no linear correlation. If the correlation coefficient is higher than 0.5, a strong quantitative correlation exists [36]. This analysis represents similarity between two measures. ICC analysis evaluates reliability between two measurement methods. ICC values range between 0 and 1, where 0–0.4 indicates poor reliability, 0.4–0.6 denotes fair, 0.6–0.75 suggests good, and 0.75–1.0 indicates excellent reliability [37]. Bland–Altman plot was used to evaluate the similarity of angle measurement between radiologist and CAD.

Results

In this study, we developed a computer-aided system that utilizes deep learning, and automatically analyzes thoracic kyphosis and lumbar lordosis. The CAD system uses VTK to depict the measured angles (Fig. 6).

Also, radiologists can select the measuring method properly between L1–L5 and L1–S (Fig. 7).

Furthermore, the performance of the segmentation model, and angle measurement algorithms were verified with the test data (60).

LAT Spine Segmentation Model Performance

Figure 8 depicts the segmented images.

The ground truth images in the test dataset and the image segmentation results were compared. Here, on an average, we observed precision of 90.53 ± 4.61%, sensitivity of 89.53 ± 1.8%, and DSC of 90.22 ± 0.62% (Table 2).

Performance of the Automated CAD Algorithm

Performance of the automatic analysis algorithms for thoracic kyphosis and lumbar lordosis was verified using the Pearson correlation and ICC analysis and additionally Bland–Altman plot which show similarities between radiologist and CAD. Manual angle measurements were determined thrice by two radiologists who have more than 10 years of experience with the same samples. No significant difference between the

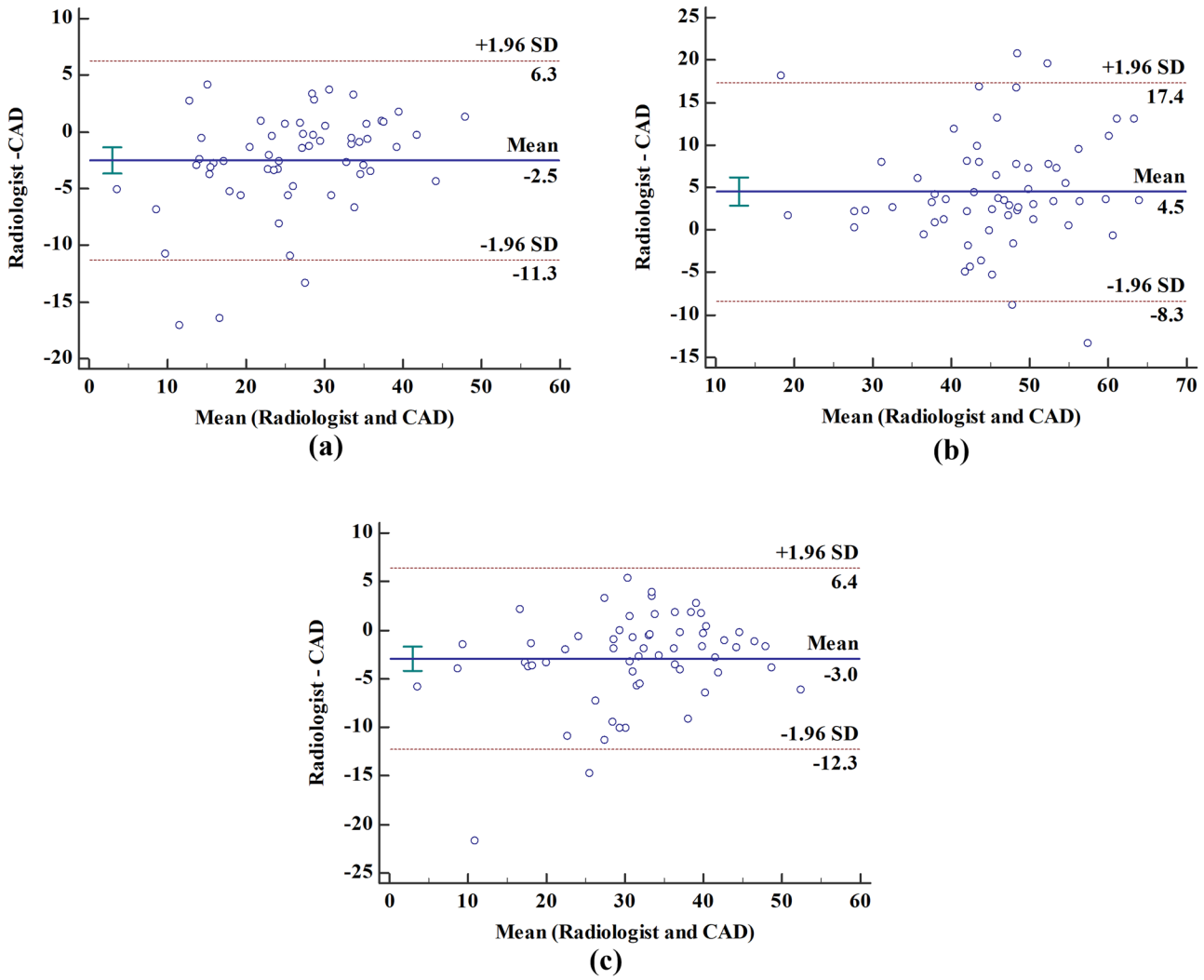

Fig. 10 Bland–Altman plots compared the angles measured by the radiologist and CAD system. **a** Thoracic kyphosis. **b** Lumbar lordosis based on L1–S. **c** Lumbar lordosis based on L1–L5

manual measurements was observed ($P > 0.05$). The Pearson correlation (R) between the values measured by the radiologist and the CAD system was 0.91 for kyphosis ($P < 0.05$), 0.80 for lordosis based on L1–S1 ($P < 0.05$), and 0.91 for lordosis based on L1–L5 ($P < 0.05$). Thus, a strong quantitative correlation was observed in all the cases. Figure 9 shows a scatter plot that depicts the similarity between two measurements. Moreover, Bland–Altman plots showed that most values were located in the 95% confidence interval, which suggested that the predicted and expected results were highly similar (Fig. 10).

Average ICC values of 0.94 for kyphosis, 0.89 for lordosis based on L1–S1, and 0.95 for lordosis based on L1–L5 were significant and reliable for all the cases (Table 3).

Table 3 ICC analyzing result table; comparison and verification of angles measured by radiologist and CAD

Spine angle	Radiologist (mean ± SD)	CAD (mean ± SD)	ICC	95% confidence interval	*P* value
Kyphosis	27.46 ± 9.26	24.95 ± 10.48	0.94	0.91–0.97	< 0.05
Lordosis (L1–S)	43.27 ± 10.43	47.78 ± 10.51	0.89	0.81–0.93	< 0.05
Lordosis (L1–L5)	32.88 ± 10.16	29.92 ± 11.16	0.95	0.91–0.97	< 0.05

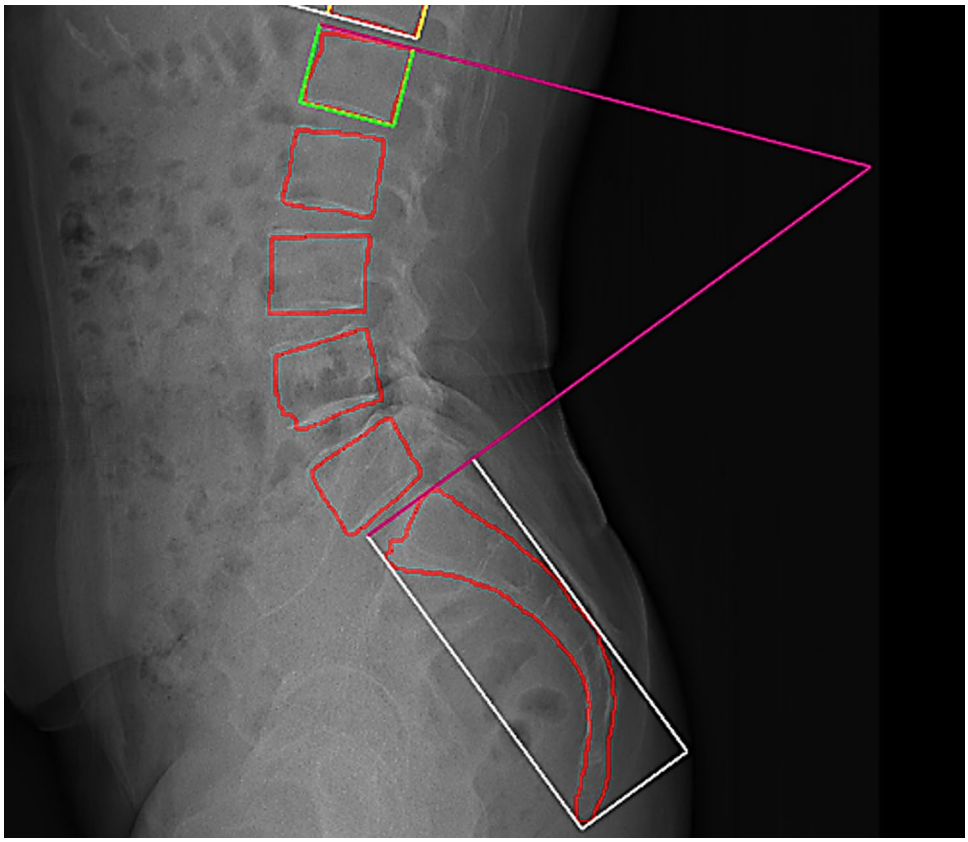

Fig. 11 The end plate of the bounding box does not match with the contour

Discussion and Conclusion

In this study, we proposed a CAD system that automatically segments vertebral contours using deep learning and analyzes thoracic kyphosis and lumbar lordosis angles based on X-ray images. The segmentation performance of the U-Net model on precision, sensitivity, and DSC values is 90% on average. However, vertebral contour detection errors were observed for some images. This may arise when images are derived from patients with congenital deformities in the spine, or due to other inclusion factors that hinder learning. Congenital vertebral anomalies, such as butterfly vertebra, hemi vertebra, and block vertebra, can affect the CAD algorithm performance, where one vertebra may be recognized as two or two vertebrae as one. Therefore, the algorithm should be modified by adding classification functions such that normal and congenital deformities can be classified before segmentation. Additionally, objects like lumbar implants and catheters inserted directly into the spine or ones that block the vertebrae can interfere with the learning process in spinal segmentation. In this respect, image processing or area-based segmentation when predicted contours overlap each other can improve the performance.

Here, we used a dataset of scoliosis patients, where the average age of patients was 62 ± 15 years. For infants and children, the boundaries of the vertebral end plate are not clear and sometimes convex in shape. Since ossification between the spinal segments is not completed until adulthood, their vertebra can have a different appearance than adults [38]. In future, reinforcement learning with additional data about infants and children can improve the developed model.

Our Bland–Altman plots show an error of typically 2–5 degrees, which is included in a tolerance error of 3–9 in clinical practice [39–41]. Sources of error are the insufficient definition of endpoint in end plate such as Fig. 11 and "divide by 0" error arising from parallel or vertical angles, etc.

This error implies that our algorithm needs further research for recognizing the end plate more precisely in the spine. In particular, unlike other vertebrae, the sacrum has an elongated triangle shape rather than a square shape. It is hard work to recognize the end plate of sacrum with just a bounding box method. Therefore, to minimize this error, we are currently further studying algorithms, such as using points at the minimum distance from the endpoint of the bounding box of the spine. It is expected that the revised algorithm can minimize measurement errors by recognizing these end plates more delicately in the future. We expect that our CAD system improves the reliability of the Cobb method in digital radiography.

An automatic angular measurement system was developed to help diagnose kyphosis and lordosis. The developed CAD system based on deep learning and mathematics

measures the kyphosis angle using T4–T12 vertebrae, and the lordosis angle using L1–S1 vertebrae, or the L1–L5. Moreover, the CAD system for measuring kyphosis and lordosis angles exhibited high similarity and reliability in comparison to radiologist's measurements. Therefore, the proposed CAD system can be useful in the clinic to diagnose spinal deformities by measuring kyphosis and lordosis angles. Furthermore, by supplementing the developed CAD algorithm with previous methods, one can help less-experienced clinicians in diagnosing spinal deformity, which can reduce the time and effort required by radiologists.

Author Contribution Kwang Gi Kim and Ji Young Jeon contributed equally in this work.

Funding This work was supported by the National Research Foundation of Korea (NRF) grant funded by the Korea government (MSIT) (No. NRF-2019R1G1A1100487), and by the MSIT (Ministry of Science and ICT), Korea, under the ITRC (Information Technology Research Center) support program (IITP-2021–2017-0–01630) supervised by the IITP (Institute for Information & communications Technology Promotion), and by the GRRC program of Gyeonggi province. [GRRC-Gachon2020(B01), AI-based Medical Image Analysis.

Availability of Data and Material Not applicable.

Code Availability Not applicable.

Declarations

Ethics Approval All procedures performed in studies involving human participants were in accordance with the ethical standards of the institutional and/or national research committee and with the 1964 Helsinki Declaration and its later amendments or comparable ethical standards. The study was approved by the institutional review board of Gachon University Gil Hospital (IRB number: GDIRB2019-137).

Consent to Participate Informed consent was obtained from all individual participants included in the study.

Consent for Publication Patients signed informed consent regarding publishing their data and photographs.

Conflict of Interest The authors declare no competing interests.

References

1. R. Izzo, G. Guarnieri, G. Guglielmi, and M. Muto: Biomechanics of the spine. Part I: Spinal stability. *Eur. J. Radiol., 82(1):118–126, 2013*. https://doi.org/10.1016/j.ejrad.2012.07.024.
2. P. Roussouly and C. Nnadi: Sagittal plane deformity: an overview of interpretation and management. *Eur. Spine J.*, 19(11):1824-1836, 2010. https://doi.org/10.1007/s00586-010-1476-9.
3. M. Dijkers: Quality of life after spinal cord injury: a meta analysis of the effects of disablement components. *Spinal Cord*, 35(12):829-840, 1997. https://doi.org/10.1038/sj.sc.3100571.
4. V. M. Ravindra *et al.*: Degenerative lumbar spine disease: estimating global incidence and worldwide volume. *Glob. Spine J.*, 8(8):784–794, 2018. https://doi.org/10.1177/2192568218770769.
5. E. K. Wai *et al.*: Quality of life in surgical treatment of metastatic spine disease. *Spine (Phila. Pa. 1976).*, 28(5):508–512, 2003. https://doi.org/10.1097/01.BRS.0000048646.26222.FA.
6. F. Schwab *et al.*: Adult scoliosis: prevalence, SF-36, and nutritional parameters in an elderly volunteer population. *Spine (Phila. Pa. 1976).*,30(9):1082–1085, 2005. https://doi.org/10.1097/01.brs.0000160842.43482.cd.
7. F. Schwab *et al.*: Scoliosis Research Society-Schwab adult spinal deformity classification: a validation study. *Spine (Phila. Pa. 1976).37(12):*1077–1082, 2012. https://doi.org/10.1097/BRS.0b013e31823e15e2.
8. M. S. Harreby *et al.*: Risk factors for low back pain in a cohort of 1389 Danish school children: an epidemiological study. *Ugeskr. Laeger*, 163(3):282–286, 2001.
9. B. Skoffer and A. Foldspang: Physical activity and low-back pain in schoolchildren. *Eur. Spine J.*, 17(3):373–379, 2008. https://doi.org/10.1007/s00586-007-0583-8.
10. W. M. Balagué F, Dutoit G: Low back pain in schoolchildren. An epidemiological study. *Scand. J. Rehabil. Med.*, 20(4):175–179, 1988.
11. E. Barrett, K. McCreesh, and J. Lewis: Intrarater and interrater reliability of the flexicurve index, flexicurve angle, and manual inclinometer for the measurement of thoracic kyphosis. *Rehabil. Res. Pract.*, 2013:1–7, 2013. https://doi.org/10.1155/2013/475870.
12. B. P. Harrison, Deed E. DC, Cailliet et al.: Reliability of Centroid, Cobb, and Harrison posterior tangent methods. *Spine (Phila. Pa. 1976).*, 26(11):e227–e234, 2001.
13. A. M. Briggs, T. V. Wrigley, E. A. Tully, P. E. Adams, A. M. Greig, and K. L. Bennell: Radiographic measures of thoracic kyphosis in osteoporosis: Cobb and vertebral centroid angles. *Skeletal Radiol.*, 36(8):761–767, 2007.
14. R. T. Morrissy, G. S. Goldsmith, E. C. Hall, D. Kehl, and G. H. Cowie: Measurement of the Cobb angle on radiographs of patients who have scoliosis. Evaluation of intrinsic error. *J. bone Jt. Surg.*, 72:320–327, 2008.
15. N. R. Dang, M. J. Moreau, D. L. Hill, J. K. Mahood, and J. Raso: Intra-observer reproducibility and interobserver reliability of the radiographic parameters in the spinal deformity study group's AIS Radiographic Measurement Manual. *Spine (Phila. Pa. 1976).*, 30(9):1064–1069, 2005. https://doi.org/10.1097/01.brs.0000160840.51621.6b.
16. [16]R. S. Alomari, V. Chaudhary, and G. Dhillon: Computer aided diagnosis system for lumbar spine. *ACM Int. Conf. Proceeding Ser.*, 2011. https://doi.org/10.1145/2093698.2093843.
17. K. Alawneh, M. Al-Dwiekat, M. Alsmirat, and M. Al-Ayyoub: Computer-aided diagnosis of lumbar disc herniation. *2015 6th Int. Conf. Inf. Commun. Syst. ICICS 2015*, no. April, pp. 286–291, 2015. https://doi.org/10.1109/IACS.2015.7103190.
18. Barron, Valerie: Generation of a finite element model of the thoracolumbar spine. *Acta of Bioengineering and Biomechanics*, 9(1):35–46, 2007.
19. M. Tiouririne, A. J. Dixon, F. W. Mauldin, D. Scalzo, and A. Krishnaraj: Imaging performance of a handheld ultrasound system with real-time computer-aided detection of lumbar spine anatomy: a feasibility study. *Invest. Radiol.*, 52(8):447–455, 2017. https://doi.org/10.1097/RLI.0000000000000361.
20. S. R. O'Connor SD, Yao JH: Lytic metastases in thoracolumbar spine: computer-aided detection at CT—preliminary study. *Radiology*, 242(3):811–816, 2007.
21. S. M. M. R. Al Arif, K. Knapp, and G. Slabaugh: Fully automatic cervical vertebrae segmentation framework for X-ray images. *Comput. Methods Programs Biomed.*, 157:95–111, 2018. https://doi.org/10.1016/j.cmpb.2018.01.006.
22. Y. J. Kim, B. Ganbold, and K. G. Kim: Web-based spine segmentation using deep learning in computed tomography images. *Healthc. Inform. Res.*, vol. 26, no. 1, pp. 61–67, 2020. https://doi.org/10.4258/hir.2020.26.1.61.

23. Y. Liu, X. Sui, C. Liu, X. Kuang, and Y. Hu: Automatic lumbar spine tracking based on Siamese convolutional network. *J. Digit. Imaging*, 33(2):423–430, 2020. https://doi.org/10.1007/s10278-019-00273-5.
24. D. Zhang, B. Chen, and S. Li: Sequential conditional reinforcement learning for simultaneous vertebral body detection and segmentation with modeling the spine anatomy. *Med. Image Anal.*, 67:101861, 2021. https://doi.org/10.1016/j.media.2020.101861.
25. B. Samuvel, V. Thomas, M. G. Mini, and J. Renjith Kumar: A mask based segmentation algorithm for automatic measurement of Cobb angle from scoliosis x-ray image. *Proc. - 2012 Int. Conf. Adv. Comput. Commun. ICACC 2012*, pp. 110–113, 2012. https://doi.org/10.1109/ICACC.2012.24.
26. M. H. Horng, C. P. Kuok, M. J. Fu, C. J. Lin, and Y. N. Sun: Cobb angle measurement of spine from x-ray images using convolutional neural network. *Comput. Math. Methods Med.*, 2019, 2019. https://doi.org/10.1155/2019/6357171.
27. R. H. Alharbi, M. B. Alshaye, M. M. Alkanhal, N. M. Alharbi, M. A. Alzahrani, and O. A. Alrehaili: Deep learning based algorithm for automatic scoliosis angle measurement. *ICCAIS 2020 - 3rd Int. Conf. Comput. Appl. Inf. Secur.*, pp. 1–5, 2020. https://doi.org/10.1109/ICCAIS48893.2020.9096753.
28. T. Long, J., Shelhamer, E. & Darrell: Fully convolutional networks for semantic segmentation. *IEEE Conf. Comput. Vis. Pattern Recognit.(CVPR) 3431–3440 (IEEE, Piscataway, NJ, USA, 2015).*
29. M. Mccormick, X. Liu, J. Jomier, C. Marion, and L. Ibanez: Itk: Enabling reproducible research and open science. *Front. Neuroinform.*, 8(FEB):1–11, 2014. https://doi.org/10.3389/fninf.2014.00013.
30. B. Schroeder, Will: Martin, Ken: *The Visualization Toolkit, 4th ed,* Lorensen: Kitware, 2006, ISBN 978–1–930934–19–1.
31. S. Noguchi, M. Nishio, M. Yakami, K. Nakagomi, and K. Togashi: Bone segmentation on whole-body CT using convolutional neural network with novel data augmentation techniques. *Comput. Biol. Med.*, 121(January):103767, 2020. https://doi.org/10.1016/j.compbiomed.2020.103767.
32. S. Kim: End-to-end bone tumor segmentation and classification from X-ray images by using multi-level Seg-Unet model. Journal of KIISE, 47(2):170–179, 2020.
33. K. Murata *et al.*: Spinal sagittal alignment in patients with dropped head syndrome. *Spine (Phila. Pa. 1976).*, 43(21):E1267–E1273, 2018. https://doi.org/10.1097/BRS.0000000000002685.
34. Stagnara P, De Mauroy JC, Dran G, Gonon GP, et al.: Reciprocal angulation of vertebral bodies in a sagittal plane: approach to references for the evaluation of kyphosis and lordosis. Spine. 7(4):335-342, 1982.
35. R. Vialle, N. Levassor, L. Rillardon: Radiographic analysis of the sagittal alignment and balance of the spine in asymptomatic subjects. *The Journal of Bone & Joint Surgery*, 87(2):260–267, 2005. https://doi.org/10.2106/00004623-200502000-00004.
36. N. J. Gogtay and U. M. Thatte: Principles of correlation analysis. Journal of The Association of Physicians of India, 65:78–81, 2017.
37. Cicchetti, Domenic V: Guidelines, criteria, and rules of thumb for evaluating normed and standardized assessment instruments in psychology. Psychological assessment, 6(4):284–290, 1994. https://doi.org/10.1037/1040-3590.6.4.284.
38. J. R. Taylor: Growth of human intervertebral discs and vertebral bodies. *J. Anat.*, 120(Pt 1):49–68, 1975.
39. M. Gstoettner, K. Sekyra, N. Walochnik: Inter- and intraobserver reliability assessment of the Cobb angle: manual versus digital measurement tools. *Eur. Spine J.*, 16(10):1587–1592, 2007. https://doi.org/10.1007/s00586-007-0401-3.
40. Amanda C.Y.Chan; Devlin G.Morrison: Intra- and interobserver reliability of the Cobb angle–vertebral rotation angle–spinous process angle for adolescent idiopathic scoliosis. *Spine Deform.*, 2(3):168–175, 2014. https://doi.org/10.1016/j.jspd.2014.02.006.
41. J. G. Carman, D L; Browne, R H; Birch: Measurement of scoliosis and kyphosis radiographs. Intraobserver and interobserver variation. *J. Bone Jt. Surg.*, 72(3):328–333, 1990.

Publisher's Note Springer Nature remains neutral with regard to jurisdictional claims in published maps and institutional affiliations.